catalysts

MDPI

Article

Galvanic Exchange as a Novel Method for Carbon Nitride Supported CoAg Catalyst Synthesis for Oxygen Reduction and Carbon Dioxide Conversion

Roshan Nazir, Anand Kumar *, Sardar Ali, Mohammed Ali Saleh Saad * and Mohammed J. Al-Marri

Department of Chemical Engineering, Qatar University, P.O. Box 2713, Doha, Qatar, Qatar; roshan.nazir@qu.edu.qa (R.N.); ali.sardar@qu.edu.qa (S.A.); m.almarri@qu.edu.qa (M.J.A.-M.)

* Correspondence: akumar@qu.edu.qa (A.K.); m.saleh@qu.edu.qa (M.A.S.S.); Tel.: +974-44034164 (A.K.)

Received: 23 September 2019; Accepted: 8 October 2019; Published: 16 October 2019

Abstract: A bimetallic alloy of CoAg nanoparticles (NPs) on a carbon nitride (CN) surface was synthesized using a galvanic exchange process for the oxygen reduction reaction (ORR) and carbon dioxide electrocatalytic conversion. The reduction potential of cobalt is ($[Co^{2+}(aq) + 2e^- \rightarrow Co(s)]$, −0.28 eV) is smaller than that of Ag ($[Ag^+(aq) + e^- \rightarrow Ag(s)]$, 0.80 eV), which makes Co(0) to be easily replaceable by Ag^+ ions. Initially, Co NPs (nanoparticles) were synthesized on a CN surface via adsorbing the Co^{2+} precursor on the surface of CN and subsequently reducing them with $NaBH_4$ to obtain Co/CN NP. The Co NPs on the surface of CN were then subjected to galvanic exchange, where the sacrificial Co atoms were replaced by Ag atoms. As the process takes place on a solid surface, only the partial replacement of Co by Ag was possible generating CoAg/CN NPs. Synthesized CoAg/CN bimetallic alloy were characterized using different techniques such as powder x-ray diffraction (PXRD), x-ray photoelectron spectroscopy (XPS), transmission electron microscopy (TEM), scanning electron microscopy (SEM), and electron diffraction spectroscopy (EDS) to confirm the product. Both the catalysts, Co/CN and CoAg/CN, were evaluated for oxygen reduction reaction in 1M KOH solution and carbon dioxide conversion in 0.5 M $KHCO_3$. In the case of ORR, the CoAg/CN was found to be an efficient electrocatalyst with the onset potential of 0.93 V, which is comparable to commercially available Pt/C having E_{onset} at 0.91 V. In the electrocatalytic conversion of CO_2, the CoAg/CN showed better performance than Co/CN. The cathodic current decreased dramatically below −0.9V versus Ag/AgCl indicating the high conversion of CO_2.

Keywords: carbon nitride; galvanic exchange; AgCo catalyst; oxygen reduction reaction; carbon dioxide conversion

1. Introduction

The use of fossil fuels for energy extraction has been convenient, though at a greater cost of CO_2 emissions. The increasing levels of carbon dioxide in the Earth's atmosphere is of serious concern that needs to be addressed. The high amounts of CO_2 in the atmosphere drastically bring changes in the temperature of the Earth's atmosphere. This problem not only increases the global temperature, but will also limit the use of fossil fuels. Alternatively, fuel cells and metal-air batteries have shown great promise for automotive industries. This is because of the fact that they work at low operating temperatures, possess high energy densities and are compatible to the environment on the basis of lower or zero harmful emissions [1–6]. Herein, this study attempts to design catalysts that are effective for clean energy production via fuel cell applications and suitable for catalytic conversion of carbon dioxide. It is a known fact that the efficiency of fuel cells and metal-air batteries are drastically affected

by the slow kinetics of the oxygen reduction reaction (ORR) at the cathode. Thus far, only Pt and noble metal-based electrocatalysts have been designed and operated in commercially available devices. These catalysts are relatively effective and efficient, however due to the lack of noble metals in the Earth's crust and high cost, a widespread commercialization of Pt based fuel cells and metal-air batteries does not seem to be feasible. Synthesizing efficient catalysts to replace Pt group metals (PGM) utilizing economical alternatives remains a critical challenge and a strategic issue for future applications. This can be achieved, to some extent, if attention is placed on the synthesis of new metal electrode support material that is able to enhance the catalytic efficiency and activity of metallic phase, without disturbing the chemical and mechanical stability. The nature of support is appreciated because it brings some interesting properties to the catalyst, such as proper dispersion of the active phase, preventing the loss of the catalyst during operation [7–11], morphological changes to increase the electrochemical active area [12–14].

Carbon nitride (CN) is a cheap, easily synthesized, photo active organic semiconductor that has displayed a remarkable performance in the field of catalysis [15]. The CN contains nitrogen atoms adjacent to carbon atoms. The interest in CN has recently increased because of the stimulated electropositivity in carbon atoms induced by the adjacent nitrogen atoms, which shows potential for the electronic interactions with various chemicals to affect their adsorption and reactivity. Due to this effect, a reduction in the activation energy barrier for oxygen adsorption and activation is expected that could possibly extend to the activation of challenging molecules, like CO_2 [16]. Lyth et al., described that in acidic solution, the onset potential of CN is 0.69 V (versus normal hydrogen electrode (NHE)) for ORR [17]. However, the reported catalytic activity for ORR is not satisfactory yet, which could be due to the weak electrical conductivity of CN [18]. Some reports suggested that graphene CN can be used as solid supports to synthesize metal and metal oxide nanoparticles (NPs) which increase the conductivity and enhance their catalytic efficiency [19–21]. The importance of using CN as a support for electrocatalytic reactions is valuable for many reasons. The presence of N-atoms in the repetitive S-triazine unit can coordinate and stabilize NPs. The nitrogen functional groups also enhance strong coordination, and the interaction between NPs and the substrate providing large and accessible sites for electron transportation [22,23]. The porous structure assists in the diffusion of reactants to the active sites and the removal of formed products from there [24].

Nanoscale silver (Ag) and silver alloys have shown good potential for catalytic applications making them a promising candidate for ORR and CO_2 reduction [25–31]. It is anticipated that ORR activity on Ag NPs takes place through a direct four-electron transfer mechanism as compared to the slow two-electron pathway by avoiding the formation of peroxide, which is a competent product in ORR [32]. However, Ag alone is not always appreciated for ORR and has proven to be less efficient than Pt on account of the strong bonding of Ag with the oxygen atom [33]. This interaction makes the O-O bond breakage less feasible on the Ag surface compared to Pt [34–36]. However, reports indicate that Ag in the presence of other metals, particularly Co to form bimetallic AgCo or alloyed AgCo, showed enhanced catalytic properties [26,27,33,37–39]. An interface containing the optimum interaction of Ag and Co binds effectively with oxygen to enhance the adsorption and subsequent reduction, possibly due to the synergistic effects induced in the presence of Co [40–43]. This effect is expected to facilitate other reactions as well, such as CO_2 reduction that this study intends to investigate along with ORR.

Considering the nature of improved catalytic properties of CoAg alloy, this study proposes to synthesize bimetallic alloy type CoAg NPs on the CN surface via galvanic exchange to combine the effects of CoAg alloying and nitrogen induced polarity in CN. The choice of galvanic exchange is based on the natural reduction potentials of Co^{+2} and Ag^{+} that are expected to easily form an alloy on the CN surface. Initially, cobalt nanoparticles are synthesized on the surface of a semiconducting CN surface using a strong reducing agent, $NaBH_4$, to form Co/CN. As the reduction of cobalt is difficult in the aqueous phase, therefore, the presence of CoO, Co_3O_4 and $Co(OH)_2$ along with cobalt nanoparticles are anticipated. The lower reduction potential of Co^{2+} compared to Ag^{+} facilitates the galvanic exchange of cobalt nanoparticles, including its oxides and hydroxides, by Ag to give CoAg/CN nanocomposites.

Both Co/CN and CoAg/CN catalysts were investigated for ORR and CO_2 reduction. As evident in the results and discussion section, the CoAg/CN shows better performance for both the reactions.

2. Results and Discussion

The preparation of bimetallic alloy type (CoAg) NPs on the CN surface via galvanic exchange is discussed in detail in the experimental section. Initially, Co/CN monometallic NPs was synthesized using a simple reduction technique and then sacrificial Co atoms were galvanically exchanged with Ag^+ to get CoAg NPs.

The structural conformity, purity and composition of the already synthesized compound were determined with the help of a powder X-ray diffraction analysis. In Figure 1, the diffraction peak at 2θ = 27.49º is associated with (002) plane of CN. The PXRD patterns of Co/CN in Figure 1 shows the peaks with 2θ = 27.49°, 33.20°, 43.71° and 59.21°. The peak with 2θ = 33.20° and 59.21° corresponds to (100) and (110) planes of $Co(OH)_2$. While the peak with 2θ = 43.71° is due to (111) crystal plane of Co nanoparticles. After galvanic exchange, CoAg, bimetallic NPs were produced. The PXRD patterns of CoAg/CN showed 2θ = 27.49°, 32.20°, 38.10°, 44.17°, 64.40°, 77.41°, and 81.62° peaks. As mentioned earlier, the peak at 27.49° belongs to the (002) plane of CN. The peak at 2θ = 32.20° represents (100) plane of $Co(OH)_2$. After galvanic exchange, there is marginal shift of 1° in $Co(OH)_2$ peak that represents (100) plane. The peak is shifted to 2θ = 32.20° from 33.20°. The other peaks of CoAg/CN correspond to (111), (200), (220), (311) and (222) Crystal planes of Ag, which corroborates with the fcc lattice structure (JCPDS 04-0783). The peak with 2θ = 43.71° due to (111) crystal plane of Co nanoparticles is not visible, which could be due to the overlap by the (200) broad peak of Ag. Furthermore, the EDS data on atomic percentage of Co and Ag shows 1.61% and 1.41% respectively, confirming close to 1:1 stoichiometry of CoAg in the sample.

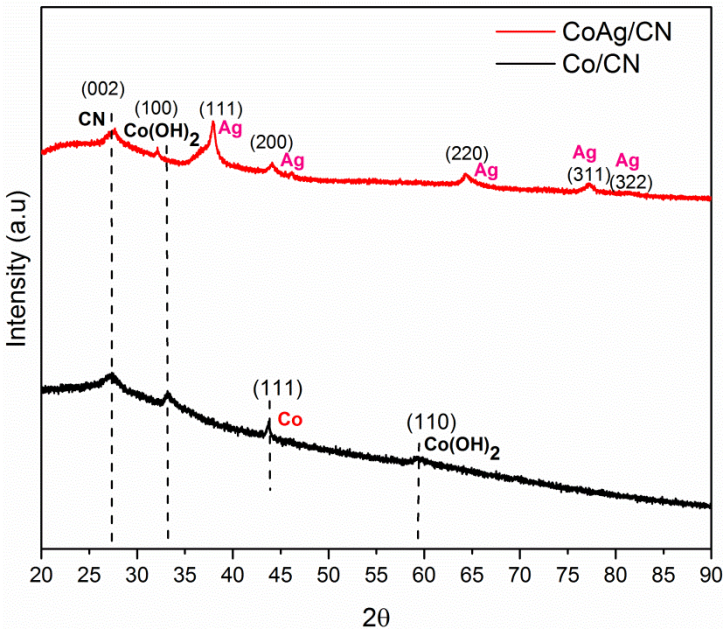

Figure 1. Powder X-ray diffraction patterns of Co/CN and CoAg/CN. During PXRD measurement, 2θ varies from 20–90° and the scanning rate was fixed at 2° per min.

Cobalt NPs are highly unstable like Fe and Ni. They were readily oxidized in aqueous medium immediately after preparation [44–46]. During the synthesis, there is a high chance of dissolved oxygen in the reaction medium. Mostly, the dissolved oxygen oxidizes the surface of cobalt. To determine the surface composition and oxidation states of the elements in CoAg/CN NPs, XPS was performed. As shown in Figure 2a, the CoAg/CN shows two core level binding energies at 780.9 eV and 796.1 eV for Co $2p_{3/2}$ and Co $2p_{1/2}$ peak, respectively. These binding energies correspond to Co^{2+} of CoO and are well matched with the literature report [47]. Another doublet with binding energies 782.7 eV and 797.6 eV for Co $2p_{3/2}$ and Co $2p_{1/2}$ peak that may be possibly due to the formation of $Co(OH)_2$ on the surface [48]. In addition, two satellite peaks are found at approximately 788.2 eV and 7984 eV, respectively. From Figure 2b, the peaks at 368.3 eV and 374.6 eV are due to the presence of $3d_{5/2}$ and $3d_{3/2}$ of Ag(0) [23], along with two Ag3d spectrum peaks at 370.9 eV and 377 eV. These two signals correspond to a shift in $3d_{5/2}$ and $3d_{3/2}$ orbitals, which infers a possible bond between the silver and oxygen atoms [49].

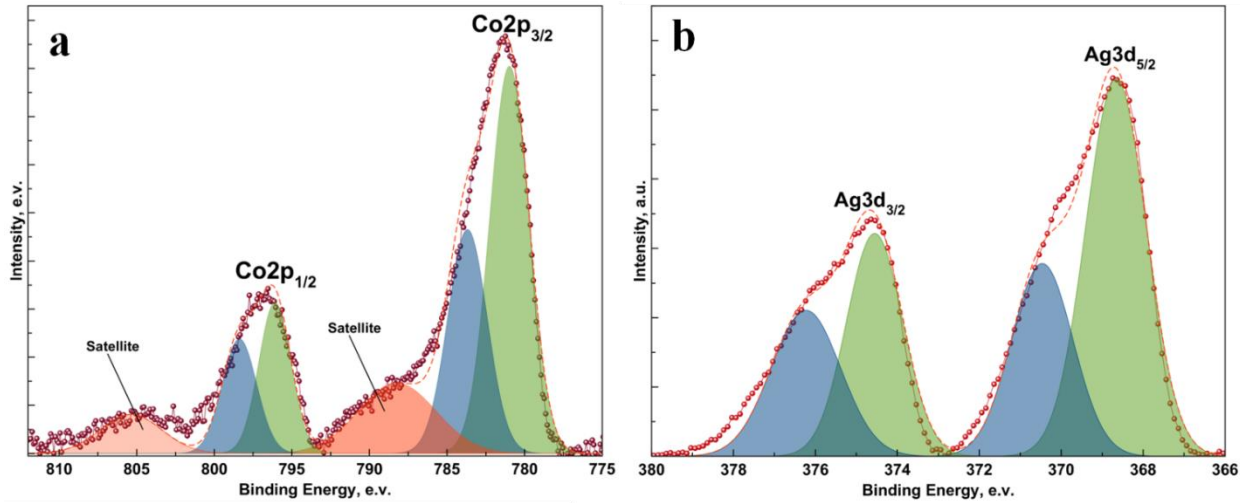

Figure 2. High-resolution deconvoluted X-ray photoelectron spectroscopy (XPS) analysis of (**a**) Co (**b**) Ag, on CN surface.

The morphologies of nanoparticles were studied by SEM techniques as shown in Figure 3. The SEM images of Co/CN and CoAg/CN are shown in Figure 3a,b respectively. As it can be seen, both Co/CN and CoAg/CNNPs seem to have a porous fibrous structure with uniform consistency of CN where the NPs are deposited. To study the crystal structure and arrangement of crystal planes, the HRTEM analysis was performed. It was confirmed from the TEM image that Co/CN NPs exhibit spherical shapes with nanoparticle >40 nm sizes, as shown in Figure 4a. The TEM image shows a near homogeneous distribution of Co particles on the CN surface. The HRTEM image of Co/CN shown in Figure 4b depicts lattice fringes of Co NPs, with an interplanar spacing 'd' = 0.203 nm corresponding to (111) plane of Co. The TEM and HRTEM of CoAg/CN are shown in Figure 4c,d, respectively. The CoAg particles appear to be spherical in nature with the size being much greater than the Co particles in Co/CN. The HRTEM image of CN/ CoAg shows interplanar spacing 'd' = 0.23 nm corresponding to (111) plane of Ag, along with 'd' = 0.203 nm that corresponds to Co as in case of Co/CN nanoparticles.

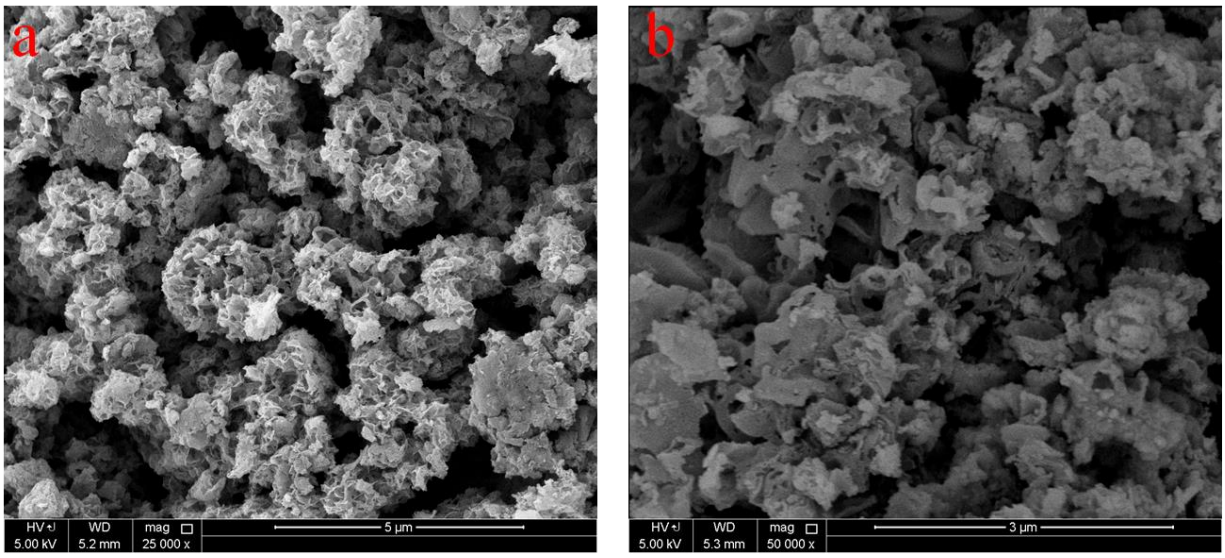

Figure 3. FESEM images of (**a**) Co/CN, (**b**) CoAg/CN.

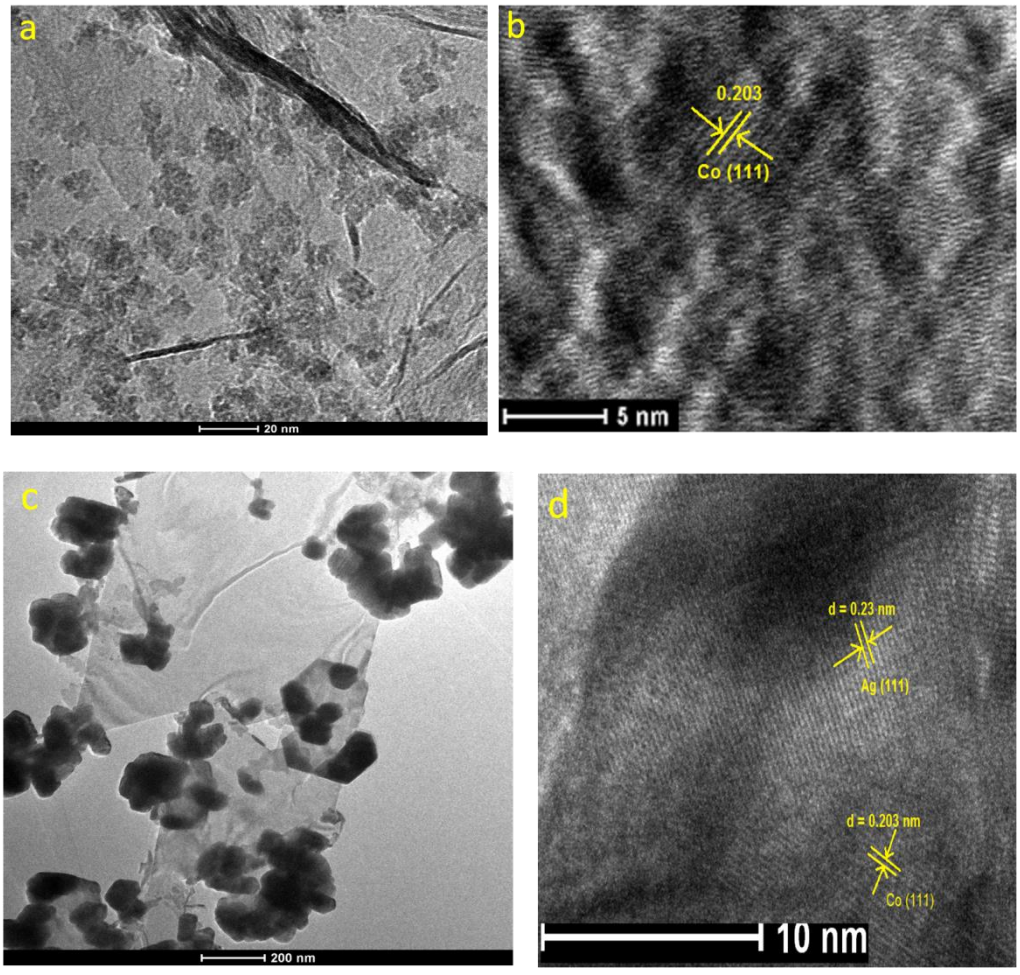

Figure 4. (**a**) TEM and high-resolution transmission electron microscopy (HRTEM) image of Co/CN. (**b**) HRTEM image shows the d-spacing calculation for Co. (**c**) TEM and (**d**) HRTEM image of CoAg/CN. HRTEM image exhibits the d-spacing calculation for Ag and Co particles.

2.1. Application in Oxygen Reduction Reactions

To check the ORR catalytic activity, Co/CN and CoAg/CN catalysts were loaded on the glassy carbon electrode. The preliminary catalytic activity of Co/CN and CoAg/CN catalysts towards the oxygen reduction reaction was studied by linear sweep voltammogram (LSV) and cyclic voltammetry (CV) techniques. The aqueous solution of 1M KOH and the scan rate of 5 mV/sec were used to study ORR activity. The experimental data collection was performed using the Ag/AgCl reference electrode to measure the potentials that were converted to potentials with respect to reversible hydrogen electrode (RHE). There was a negligible response from the bare GCE in the potential window used in this study. Figure 5 shows the LSV diagram for Co/CN and CoAg/CN catalysts in the nitrogen and oxygen saturated solution. From the LSV curves, it is clear (Figure 5a,b) that there is no peak in the nitrogen saturated solution. Both, Co/CN and CoAg/CN exhibit a remarkable increase in the current density in the presence of oxygen that is accompanied by successive anodic shifts in the onset potential. By comparing the ORR activity of Co/CN and CoAg/CN, the LSV polarization curves indicate that CoAg/CN performs better than Co/CN.

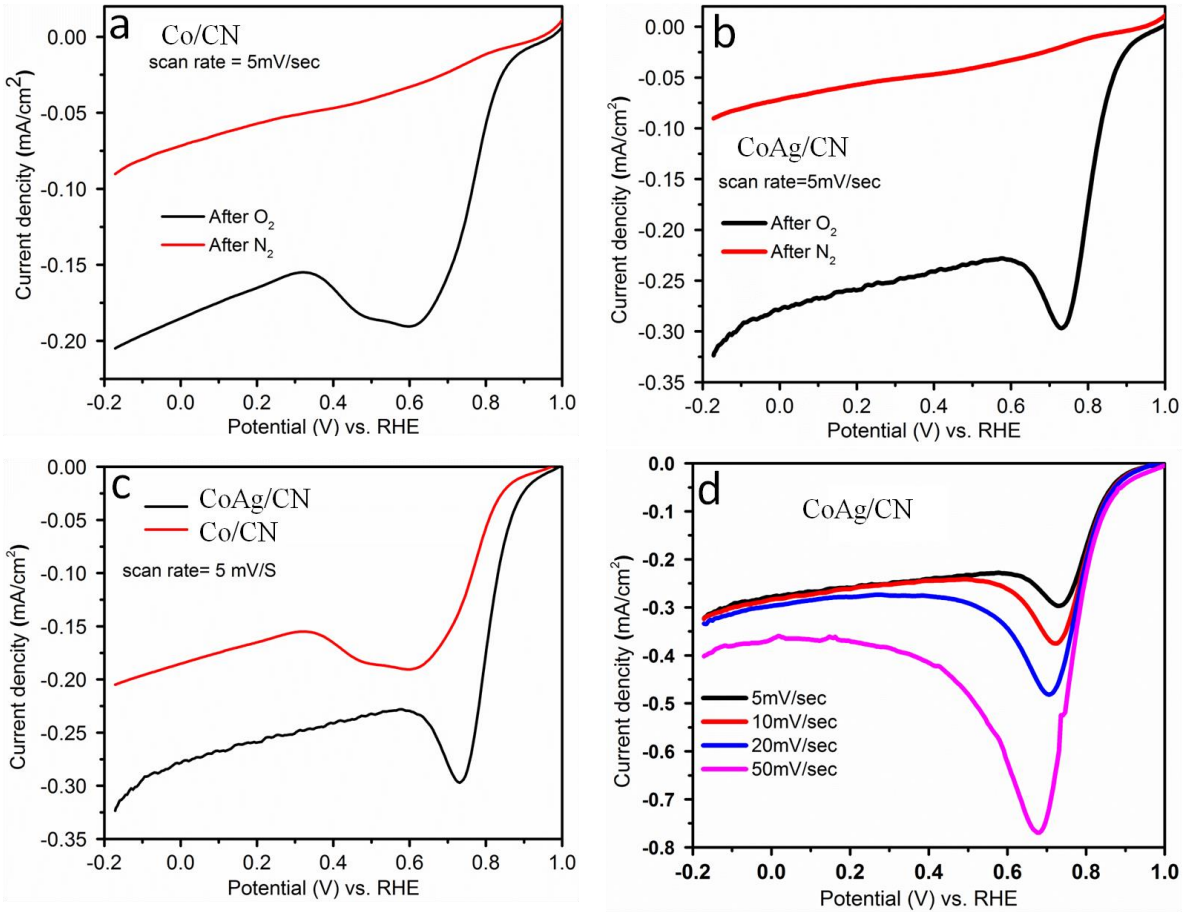

Figure 5. (**a**) Linear sweep voltammogram curve of Co/CN after N_2 and O_2 purge; (**b**) Linear sweep voltammogram curve (LSV) of CoAg/CN after N_2 and O_2 purge; (**c**) LSV comparison of Co/CN and CoAg/CN at a scan rate of 5mV/sec; (**d**) LSV polarization curves of CoAg/CN at different scan rates.

The onset potential (E_{onset}) of Co/CN and CoAg/CN are 0.89 V and 0.93 V, respectively. The activity of CoAg/CN is comparable to commercially available Pt/C with E_{onset} is 0.91 V. The LSV polarization curves in Figure 5d reveal that there is an increase in the current density with an increase in the scan rate. The cyclic voltammetry (CV) diagrams for the two electrodes (Figure 6a,b) show that the reduction peaks are absent under N_2 saturated conditions. While after purging with oxygen, the reduction peak in the case of Co/CN was at 0.47 V, while for the CoAg/CN, the reduction peak appeared at

approximately 0.7 V. By comparing Co/CN with CoAg/CN (Figure 6c), the reduction peak for CoAg/CN is more intense and shows an increase in the current density. This better activity of CoAg/CNwith respect to Co/CN was also observed with the rotating ring disc cyclic voltammetry (RRDCV). The scan rate 5 mV/sec with a rotating speed 1500 rpm were the parameters taken to run RRDCV for Co/CN with CoAg/CN electrodes. The information from RRDCV (Figure 7) also infers better ORR activity of CoAg/CN than Co/CN. The better activity of CoAg/CN with respect to Co/CN may be due to the synergistic effect of Co and Ag alloy type nanoparticles. The literature reports also convey that the synergistic effect is not only responsible for better activity, but the galvanic exchange approach modifies the surface to enhance the electron transfers [23]. It is quite evident that during galvanic exchange, there are surface modifications, such as voids, which are formed and probably make the galvanic exchange material better electrocatalysts [23,50]. Compared with Pt, Hoon and co-workers have mentioned that the E_{onset} of commercially is 0.91V for ORR, which indicates CoAg/CN to have a comparable onset potential of 0.93V [51].

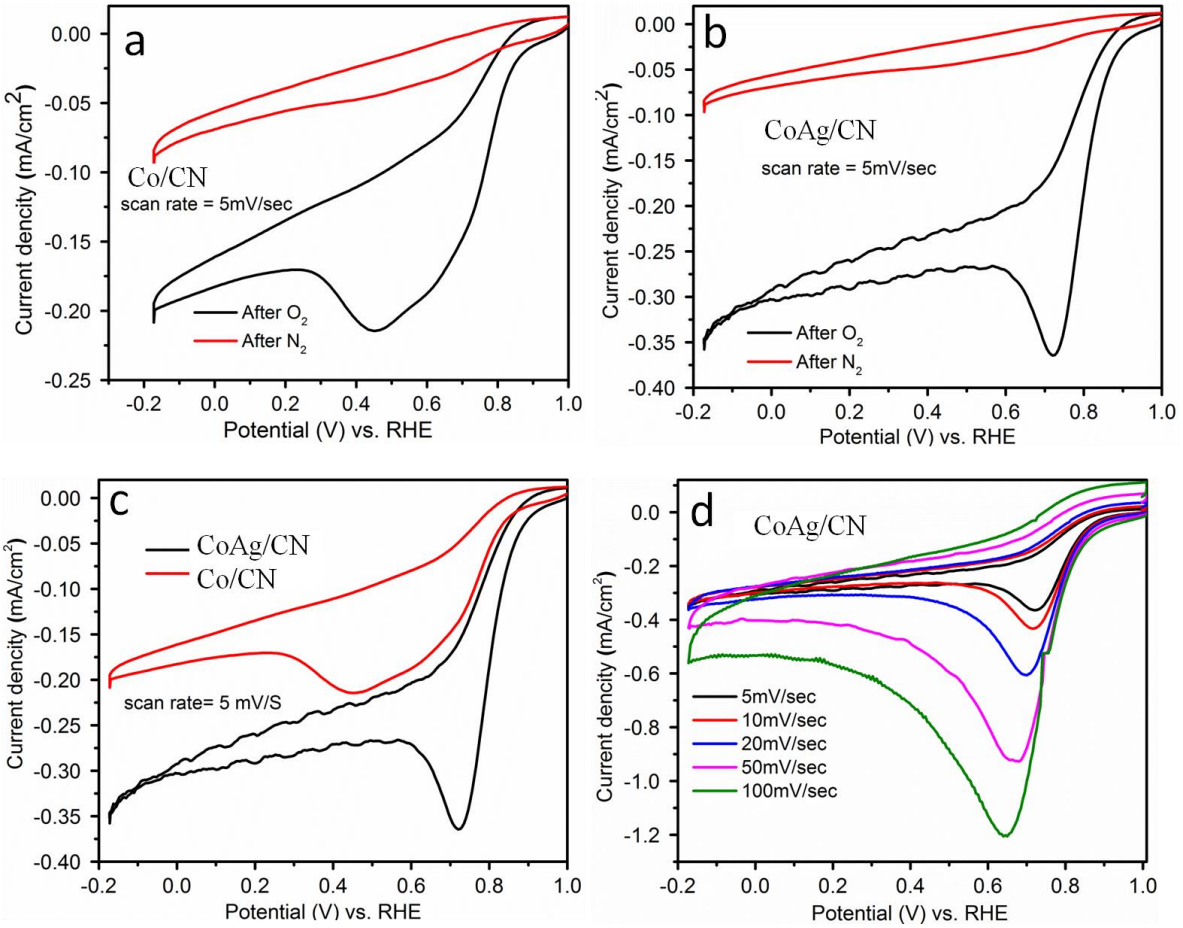

Figure 6. (**a**) Cyclo voltammogram diagram of Co/CN after N_2 and O_2 purge. (**b**) Cyclo voltammogram of CoAg/CN after N_2 and O_2 purge. (**c**) CV comparison of Co/CN and CoAg/CN at scan rate of 5mV/sec (**d**) CV of CoAg/CN at different scan rates.

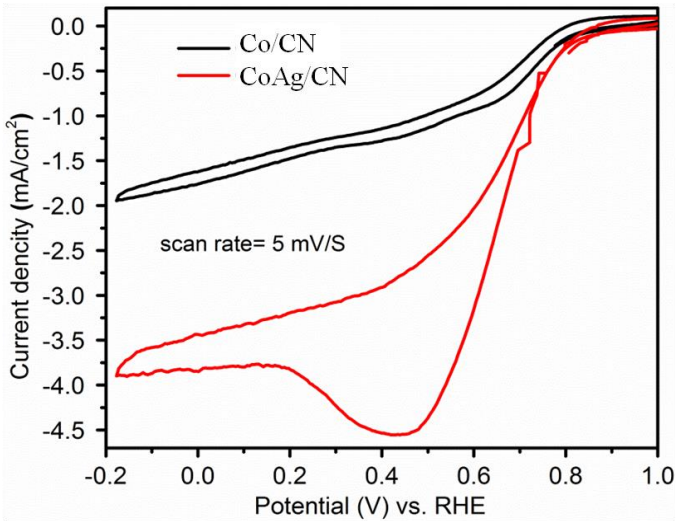

Figure 7. Rotating ring disc cyclic voltammetry (RRDCV) comparison of Co/CN and CoAg/CN scan rate 5mV/sec with rotating speed 1500 rpm.

2.2. Application in Carbon Dioxide Conversion

Both the Co/CN and CoAg/CN electrodes were also evaluated for electrocatalytic conversion of carbon dioxide. The CV scans of Co/CN and CoAg/CN electrodes with the RDE disc electrode were scanned between 0.8 and −1.2 V versus Ag/AgCl in 0.5 M $KHCO_3$ solution at 100mV/sec scan rate. Figure 8a CV scans show the redox peaks at 0.08 and −0.3 V on the forward and reverse scans, respectively. It is quite clear that the cathodic current increases dramatically after −0.9 V in CO_2 saturated solution, as compared to N_2 saturation where not much activity is seen. The results reveal that there is an active utilization of electrons supplied to the cathode during CO_2 uptake. Figure 8b shows the redox peaks at −0.23, 0.35 on forward −0.13 and −0.9 V on reverse scans, respectively. The number of peaks increased after the CO_2 purge in the forward scan and there is clear sudden jump at approximately −0.9 V in the reverse scan. The reduction peak in the region −0.9 to −1 V indicates the carbon dioxide reduction. Figure 9 compares the activity of Co/CN and CoAg/CN electrodes under CO_2 saturated conditions and clearly depicts the superior performance of CoAg/CN as an active catalyst compared to Co/CN. The current density at −1.2 V jumps to 1.5mV/cm^2 for CoAg/CN, almost three times the value for Co/CN, which is 0.55 mA/cm^2. The nature of the product formed on the surface of the disc electrode was estimated by using RRDE and matching with the oxidation potential of the expected products on the Pt (ring electrode) surface. This analysis was conducted only on the CoAg/CN electrode on the basis of higher activity and expectedly larger amounts of products that can be detected using the ring electrode. As the total amount of active phase on the disc electrode is extremely small, a reasonable amount of product should be present to be detected on the ring electrode. The CoAg/CN electrodes were scanned between 0 and −1.2 V versus RHE, and the ring electrode was held at 0.9 V versus RHE, which is the reported oxidation potential of formic acid on the Pt surface [52]. Figure 10 shows an initial CV scan for the N_2 purged electrolyte and Figure 10b shows the CV for the CO_2 purged electrolyte. The CV graph in Figure 10b reveals that there is an increase in the current density in both the ring and disc currents after purging the CO_2. There is also a peak (Figure 10b) at −0.9 V that corresponds to the formation of formic acid as indicated by a peak in the ring electrode current density. X. Zhu et al. did a series of experiments while scanning the ring electrode between 0 and 1.3 V keeping the disc electrode at −0.4, −0.5. −0.6, −0.7, −0.8 and −0.9 V [52]. They concluded that when the disc electrode is kept at a potential of −0.9 V, there is maximum intensity in the oxidation peak due to the conversion of carbon dioxide into formic acid at −0.9 V. The role of the ring electrode here is to oxidize the product formed due to CO_2 conversion. In order to maximize the product form, the disc electrode was kept at −0.9 V and the Pt-ring electrode was scanned between 0 and 1.3V to examine the oxidation potential of the product generated on the disc electrode. As shown in Figure 11, an oxidation

peak at 0.9 V is observed, which indicates the conversion of CO_2 to formic acid on the CoAg/CN surface [43]. Figure 12 shows a possible reaction pathway for CO_2 conversion on the CoAg/CN surface. The CO_2 molecules initially get adsorbed on the surface of the catalyst. The electron supplied by the by the cathode transforms CO_2 molecules to carbonate anion, which in the presence of a proton and an electron get converted to bicarbonate ion [8]. The bicarbonate ion in the presence of H^+ is converted to formic acid and desorbs from the surface of the catalyst.

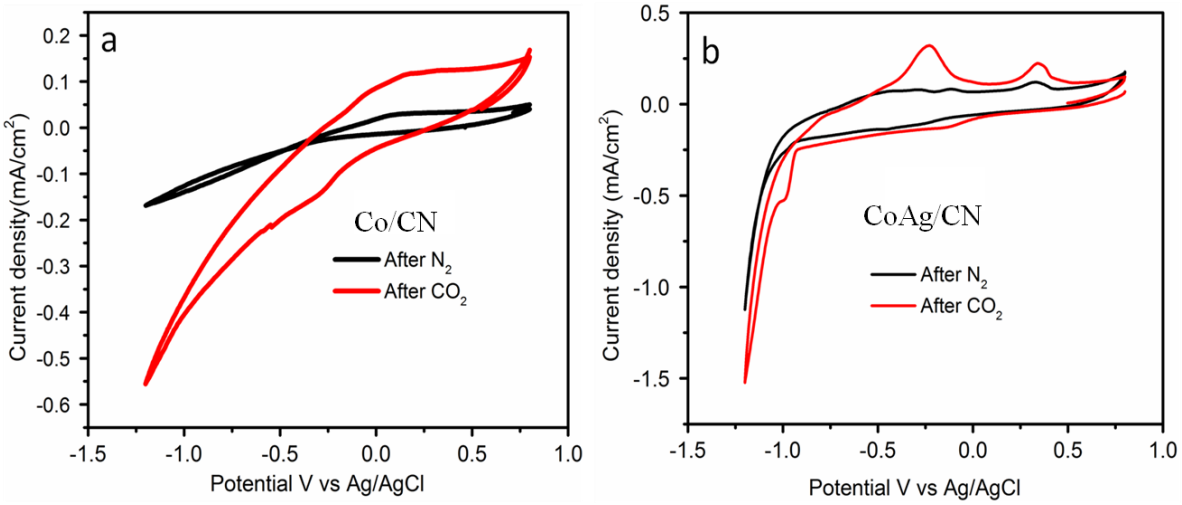

Figure 8. (**a**) CV of Co/CN in 0.5 M $KHCO_3$ after N_2 and CO_2 purge (**b**) CV of CoAg/CN in 0.5 M $KHCO_3$ after N_2 and CO_2 purge.

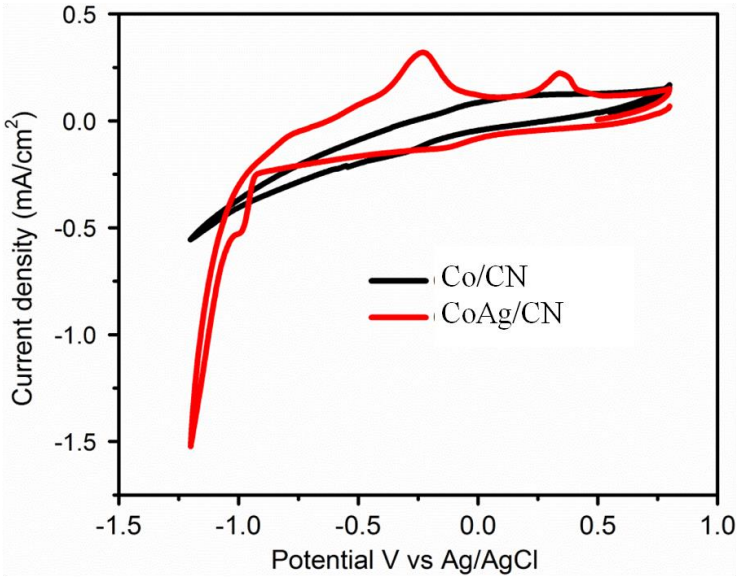

Figure 9. CV Comparison of CoAg/CN and Co/CN in 0.5 M $KHCO_3$ at a scan rate of 100mV/sec after CO_2 purge.

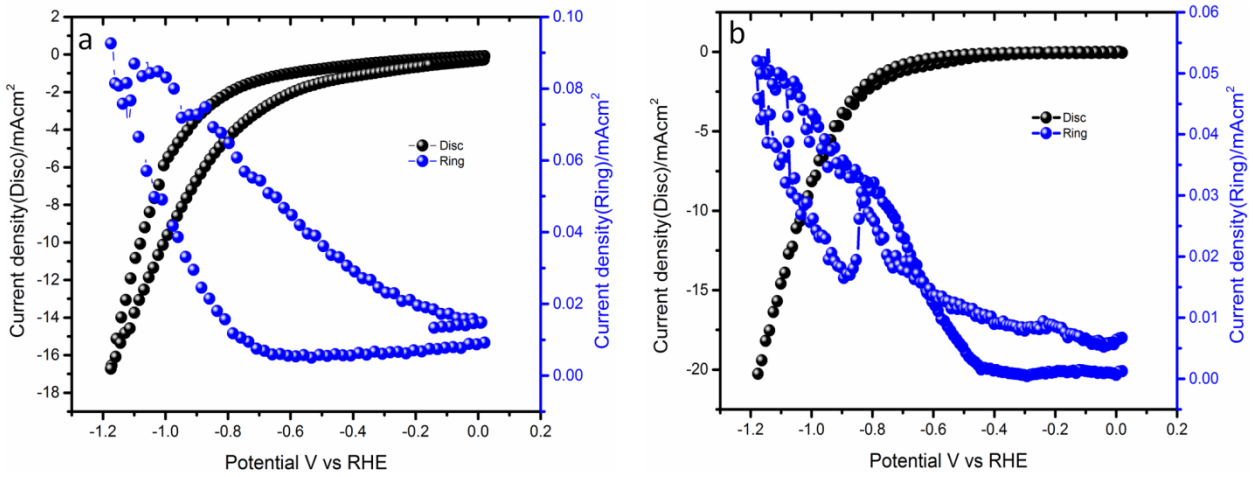

Figure 10. Cyclic voltammetry scans of CoAg/CN with RRDE. Disc electrode was scanned between 0 and −1.2 V versus RHE, the ring electrode was held at 0.9 V versus RHE. (**a**) Initial CV scan for N_2 purged electrolyte. Ring electrode was held at 0.9 V versus RHE. (**b**) CV scan for the system after CO_2 saturation with the ring held at 0.9 V versus RHE. The experiments were all performed at room temperature. Scan rate: 100 mV s^{-1}. Constant rotation (1500 rpm) was used.

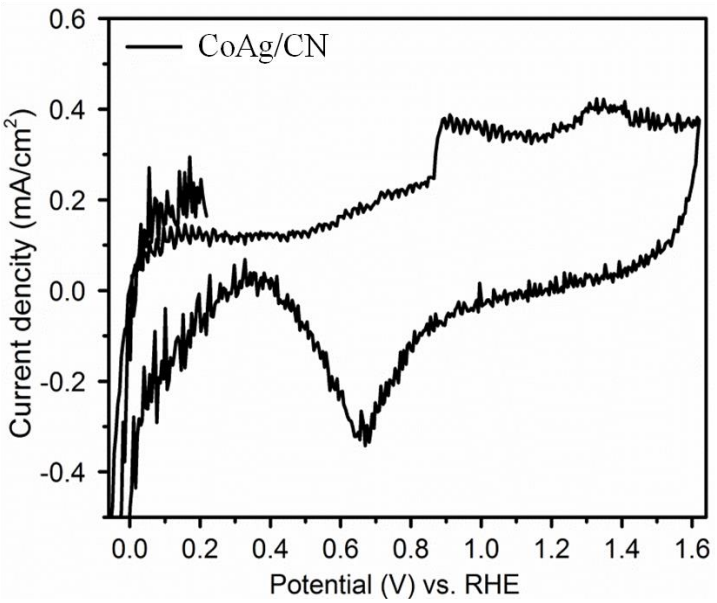

Figure 11. Cyclic voltammetry scan CoAg/CN of the ring electrode when the disc electrode was held at −0.9 V versus RHE. Ring electrode was scanned between 0 and 1.3 V versus RHE. A constant rotation of 1500 rpm was applied in each case. Scan rate: 100mV s^{-1}.

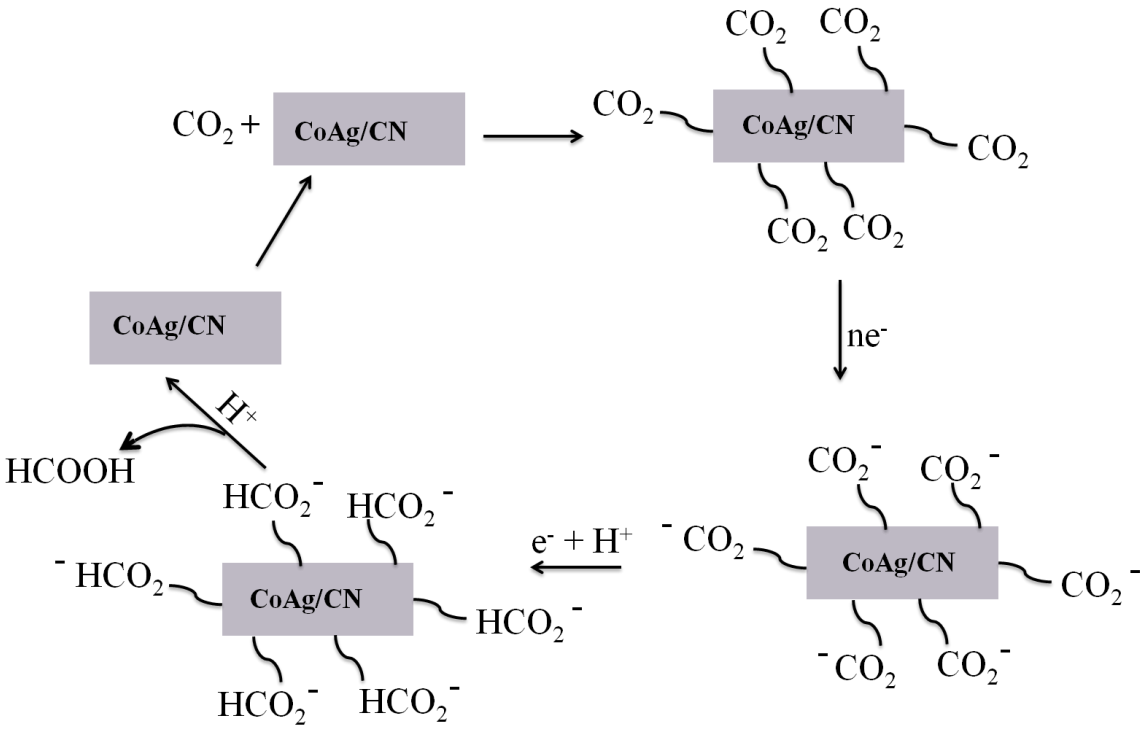

Figure 12. Possible mechanism of CO_2 conversion to HCOOH on the CoAg/CN surface.

3. Experimental Section

All the chemicals were used as received from the supplier without any further purifications. Urea in its purest form was purchased from Bio-Red laboratories. $AgNO_3$ (99.8%) was purchased from Samchun chemicals. $Co(NO_3)_2{\cdot}6H_2O$ (98%), $NaBH_4$ (98%), perfluorinated nafion, isopropyl alcohol were purchased from Sigma-Aldrich. Millipore water was used in all our experiments.

3.1. Synthesis of Carbon Nitride

The synthesis of CN was carried out by following the procedure mentioned in the literature [53,54]. CN in a powdered form was obtained by heating urea for 3 h at 550 °C. Initially, the carbon and nitrogen rich urea (10 g) was dried in a water bath. The dried urea was transferred in a ceramic crucible covered with a lid and placed inside a muffle furnace that was set at 550 °C. After 3 h of heating, a CN (a yellow colored powder) was obtained, which was cleaned with 0.1 M nitric acid and then dried at 80 °C for 30 min.

3.2. Synthesis of Co/CN

Further, 40 mg of CN powder was sonicated in 40 mL water for 15 min. Cobalt nitrate hexahydrate (0.116 g) was added in the solution to make the final concentration of the solution 10^{-2} M. The mixture was stirred for 2 h, and thereafter 0.151 g of $NaBH_4$ was slowly added to the reaction mixture. The stirring was continued for the next 3 h. Finally, the mixture was separated, cleaned 3 times with water and 1 time with ethanol in order to remove the impurities. After this procedure, the powder was dried at 80 °C for 1 h to get Co/CN powder.

3.3. Synthesis of CoAg/CN Bimetallic NPs

The galvanic approach was applied to synthesize the bimetallic NPs from Co/CN monometallic NPs. A 20 mg of synthesized Co/CN powder was added in a beaker containing silver nitrate solution (10 mL of 10^{-2} M). The mixture was sonicated for 15 min. A change in color, from green to black, was observed during the addition of Co/CN NPs. After sonication, the mixture was stirred for 1 h. Then,

the product was subjected to cleaning, 3 times with water and 1 time with ethanol, in order to remove the impurities. After this procedure, the powder was dried at 80 °C for 1h to get CoAg/CN powder. The overall synthetic procedure is shown in Scheme 1a.

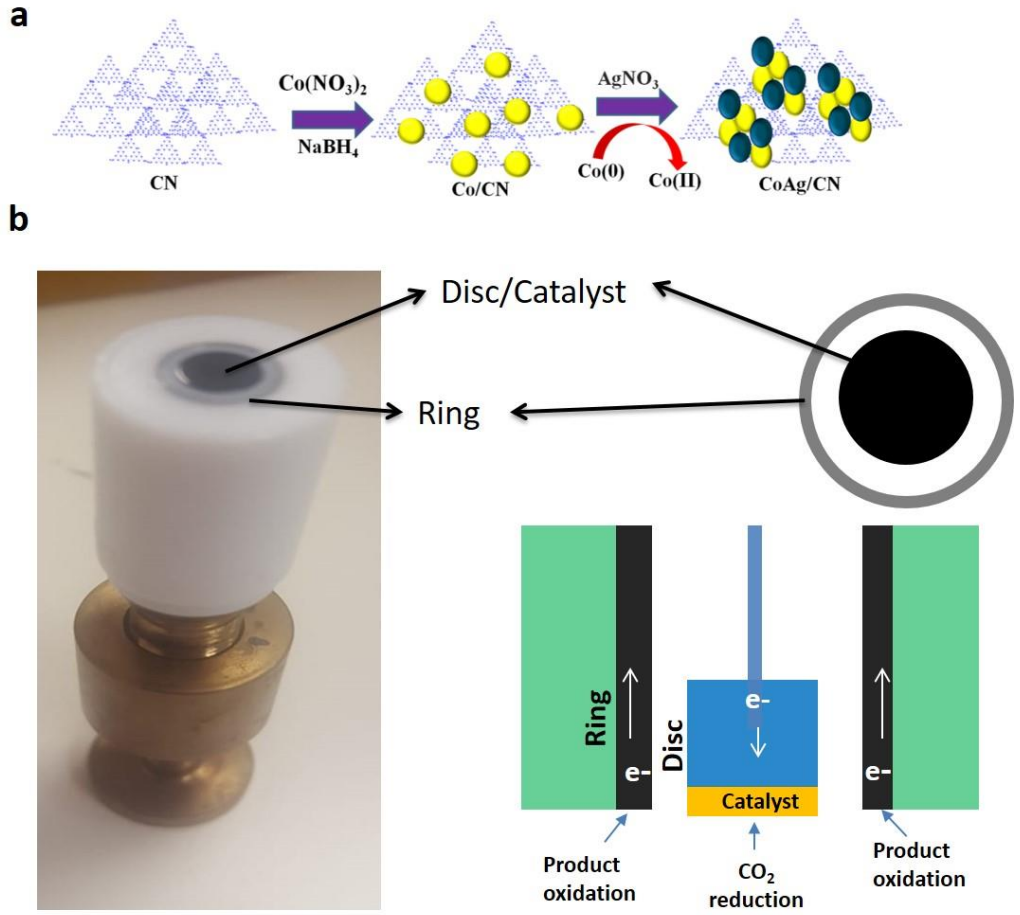

Scheme 1. (**a**) Schematic representation for the synthesis of Co and CoAg bimetallic nanoparticles on a carbon nitride (CN) surface via galvanic exchange. (**b**) Schematic of the rotating ring disc electrode (RRDE) used for the carbon dioxide electrocatalytic reduction.

3.4. Characterization Techniques

Powder X-ray diffraction measurements were performed with a Rigaku Mini Flex II Desktop X-ray powder diffractometer (Rigaku, Leatherhead, UK) with Cu-Kα radiation at 25 °C to determine the crystallinity of Co/CN and CoAg/CN nanocomposites. PXRD was recorded using 2θ = 10–80° with 2° per min scan rate. To check the surface morphology, a scanning electron microscope (Nova Nano 450, FEI Waltham, MA, USA), with magnification up to 200 kx was used. The TEM analysis was performed using a high-resolution transmission electron microscopy (HRTEM, TECNAI G^2). The carbon coated copper grids with 400-mesh were used during sample preparation. A mixture of water/ethanol solution was used to prepare the dispersed solution of the samples by sonicating them for 30 min. A 20 µL volume of the dispersed solution was drop casted on the surface of the TEM grid and dried before using in the electron microscope. X-ray photoelectron spectroscopy (XPS, Kratos AXIS Ultra DLD, Manchester, UK) was used to analyze the surface composition and oxidation states of the elements in the synthesized NPs.

3.5. Electrode Preparation

An ink containing 3mg of the catalyst 100 µL of isopropyl alcohol, 40µL nafion solution and 40 µL of DIW was prepared for electrocatalytic activity measurements of the NPs. The mixture was taken in a 20 mL of a glass vial and sonicated for 15 min. A 5 µL of ink was drop casted on GCE (PINE Research Instruments, RDE, d = 5.0 mm and geometric area, A = 0.196 cm^2). The oxygen saturated 1M KOH was used as an electrolyte during electrochemical measurements for ORR, whereas a 0.5M $KHCO_3$ saturated with CO_2 was used for CO_2 conversion studies. The details of the scan rate and applied voltage are provided in the results and discussion section to avoid repetition. A rotating ring disc electrode (RRDE) assembly was used to conduct the electrocatalytic conversion reaction of carbon dioxide. A schematic of the RRDE assembly is shown in Scheme 1b, whereas a detailed description is provided in the results and discussion section.

4. Conclusions

A bimetallic alloy of CoAg was synthesized on the CN surface via a galvanic exchange process. First, the Co NPs were synthesized on the CN surface using $NaBH_4$, a strong reducing agent. The Co NPs were used as sacrificial atoms to be replaced by Ag NPs because of the low reduction potential of Co^{2+} as compared to Ag^+. The electrocatalytic performance of both the catalysts, Co/CN and CoAg/CN, were evaluated for oxygen reduction reaction and carbon dioxide conversion. The CoAg/CN catalyst showed superior performance than Co/CN, for both ORR and CO_2 conversion reactions. The RRDE experiments indicate the reduction of CO_2 to formic acid on the CoAg/CN surface. The higher activity of CoAg/CN than Co/CN is credited to the synergistic effect of the alloy type CoAg NPs and the change in surface morphology of CoAg/CN during the galvanic exchange process.

Author Contributions: R.N.: Data acquisition, analysis and writing the first draft, A.K.: funding acquisition, supervision, review and editing, S.A.: characterization, review and editing, M.A.S.S.: review and editing, M.J.A.-M.: review and editing.

Funding: This research was funded by Total Research & Technology Feluy (grant number: QUEX-CENG-TRT-17/18).

Acknowledgments: The authors would like to gratefully acknowledge financial support from Total Research & Technology Feluy (Grant Number: QUEX-CENG-TRT-17/18) in conducting this research. The statements made herein are solely the responsibility of the authors. The authors also wish to gratefully acknowledge the Gas Processing Centre (GPC) at Qatar University for carrying out XRD and XPS analysis, and the Central Laboratory Unit (CLU) at Qatar University for services related to electron microscopy.

Conflicts of Interest: The authors declare no conflict of interest.

References

1. Mayrhofer, K.J.; Arenz, M. Fuel cells: log on for new catalysts. *Nat. Chem.* **2009**, *1*, 518. [CrossRef] [PubMed]
2. Jung, H.; Hassoun, J.; Park, J.; Sun, Y.; Scrosati, B. An improved high-performance lithium–air battery. *Nat. Chem.* **2012**, *4*, 579. [CrossRef] [PubMed]
3. Matin, M.A.; Kumar, A.; Saad Saleh, M.A.H.; Al-Marri, M.J.; Suslov, S. Zn-enriched PtZn nanoparticle electrocatalysts synthesized by solution combustion for ethanol oxidation reaction in an alkaline medium. *MRS Commun.* **2018**, *8*, 411–419. [CrossRef]
4. Matin, M.; Kumar, A.; Bhosale, R.; Saad, M.S.; Almomani, F.; Al-Marri, M. PdZn nanoparticle electrocatalysts synthesized by solution combustion for methanol oxidation reaction in an alkaline medium. *RSC Adv.* **2017**, *7*, 42709–42717. [CrossRef]
5. Ashok, A.; Kumar, A.; Bhosale, R.R.; Almomani, F.; Malik, S.S.; Suslov, S.; Tarlochan, F. Combustion synthesis of bifunctional $LaMO_3$ (M=Cr, Mn, Fe, Co, Ni) perovskites for oxygen reduction and oxygen evolution reaction in alkaline media. *J. Electroanal. Chem.* **2018**, *809*, 22–30. [CrossRef]
6. Ashok, A.; Kumar, A.; Bhosale, R.; Almomani, F.; Saad, M.A.H.S.; Suslov, S.; Tarlochan, F. Influence of fuel ratio on the performance of combustion synthesized bifunctional cobalt oxide catalysts for fuel cell application. *Int. J. Hydrog. Energy* **2019**, *44*, 436–445. [CrossRef]

7. Liu, C.; Wei, Y.; Wang, K. Surface condition manipulation and oxygen reduction enhancement of PtAu/C catalysts synergistically modified by CeO_2 addition and N_2 treatment. *J. Phys. Chem. C* **2011**, *115*, 8702–8708. [CrossRef]
8. Favaro, M.; Agnoli, S.; Perini, L.; Durante, C.; Gennaro, A.; Granozzi, G. Palladium nanoparticles supported on nitrogen-doped HOPG: a surface science and electrochemical study. *Phys. Chem. Chem. Phys.* **2013**, *15*, 2923–2931. [CrossRef]
9. Wolf, E.; Kumar, A.; Mukasyan, A. Combustion synthesis: a novel method of catalyst preparation. *Catalysis* **2019**, *31*, 297–346.
10. Kumar, A. Current trends in cellulose assisted combustion synthesis of catalytically active nanoparticles. *Ind. Eng. Chem. Res.* **2019**, *58*, 7681–7689. [CrossRef]
11. Ashok, A.; Kumar, A.; Tarlochan, F. Preparation of Nanoparticles via Cellulose-Assisted Combustion Synthesis. *Int. J. Self-Propagating High-Temp. Synth.* **2018**, *27*, 141–153. [CrossRef]
12. Perini, L.; Durante, C.; Favaro, M.; Agnoli, S.; Granozzi, G.; Gennaro, A. Electrocatalysis at palladium nanoparticles: Effect of the support nitrogen doping on the catalytic activation of carbonhalogen bond. *Appl. Catal. B Environ.* **2014**, *144*, 300–307. [CrossRef]
13. Leiva, E.; Iwasita, T.; Herrero, E.; Feliu, J.M. Effect of adatoms in the electrocatalysis of HCOOH oxidation. A theoretical model. *Langmuir* **1997**, *13*, 6287–6293. [CrossRef]
14. Smith, S.P.; Abruña, H.D. Structural effects on the oxidation of HCOOH by bismuth modified Pt (111) electrodes with (110) monatomic steps. *J. Electroanal. Chem.* **1999**, *467*, 43–49. [CrossRef]
15. Fu, X.; Hu, X.; Yan, Z.; Lei, K.; Li, F.; Cheng, F.; Chen, J. Template-free synthesis of porous graphitic carbon nitride/carbon composite spheres for electrocatalytic oxygen reduction reaction. *Chem. Commun.* **2016**, *52*, 1725–1728. [CrossRef]
16. Zhang, L.; Su, Z.; Jiang, F.; Yang, L.; Qian, J.; Zhou, Y.; Li, W.; Hong, M. Highly graphitized nitrogen-doped porous carbon nanopolyhedra derived from ZIF-8 nanocrystals as efficient electrocatalysts for oxygen reduction reactions. *Nanoscale* **2014**, *6*, 6590–6602. [CrossRef]
17. Lyth, S.M.; Nabae, Y.; Moriya, S.; Kuroki, S.; Kakimoto, M.; Ozaki, J.; Miyata, S. Carbon nitride as a nonprecious catalyst for electrochemical oxygen reduction. *Phys. Chem. C* **2009**, *113*, 20148–20151. [CrossRef]
18. Zhang, Y.; Mori, T.; Ye, J.; Antonietti, M. Phosphorus-doped carbon nitride solid: enhanced electrical conductivity and photocurrent generation. J. *Am. Chem. Soc.* **2010**, *132*, 6294–6295. [CrossRef]
19. Darabdhara, G.; Amin, M.A.; Mersal, G.A.; Ahmed, E.M.; Das, M.R.; Zakaria, M.B.; Malgras, V.; Alshehri, S.M.; Yamauchi, Y.; Szunerits, S. Reduced graphene oxide nanosheets decorated with Au, Pd and Au–Pd bimetallic nanoparticles as highly efficient catalysts for electrochemical hydrogen generation. *J. Mater. Chem. A* **2015**, *3*, 20254–20266. [CrossRef]
20. Krishnamurthy, S.; Kamat, P.V. Galvanic exchange on reduced graphene oxide: designing a multifunctional two-dimensional catalyst assembly. *J. Phys. Chem. C* **2012**, *117*, 571–577. [CrossRef]
21. Bhowmik, T.; Kundu, M.K.; Barman, S. Palladium nanoparticle–graphitic carbon nitride porous synergistic catalyst for hydrogen evolution/oxidation reactions over a broad range of pH and correlation of its catalytic activity with measured hydrogen binding energy. *ACS Catal.* **2016**, *6*, 1929–1941. [CrossRef]
22. Perini, L.; Durante, C.; Favaro, M.; Perazzolo, V.; Agnoli, S.; Schneider, O.; Granozzi, G.; Gennaro, A. Metal–support interaction in platinum and palladium nanoparticles loaded on nitrogen-doped mesoporous carbon for oxygen reduction reaction. *ACS Appl. Mater. Interfaces* **2015**, *7*, 1170–1179. [CrossRef] [PubMed]
23. Nazir, R.; Fageria, P.; Basu, M.; Pande, S. Decoration of carbon nitride surface with bimetallic nanoparticles (Ag/Pt, Ag/Pd, and Ag/Au) via galvanic exchange for hydrogen evolution reaction. *J. Phys. Chem. C* **2017**, *121*, 19548–19558. [CrossRef]
24. Nazir, R.; Fageria, P.; Basu, M.; Gangopadhyay, S.; Pande, S. Decoration of Pd and Pt nanoparticles on a carbon nitride (C 3 N 4) surface for nitro-compounds reduction and hydrogen evolution reaction. *New J. Chem.* **2017**, *41*, 9658–9667. [CrossRef]
25. Taşcı, Z.; Kunduracıoğlu, A.; Kani, İ.; Çetinkaya, B. A New Application Area for Ag-NHCs: CO_2 Fixation Catalyst. *ChemCatChem* **2012**, *4*, 831–835. [CrossRef]
26. Ashok, A.; Kumar, A.; Tarlochan, F. Surface alloying in silver-cobalt through a second wave solution combustion synthesis technique. *Nanomaterials* **2018**, *8*, 604. [CrossRef]

27. Ashok, A.; Kumar, A.; Matin, M.A.; Tarlochan, F. Synthesis of highly efficient bifunctional Ag/Co_3O_4 catalyst for oxygen reduction and oxygen evolution reactions in alkaline medium. *ACS Omega* **2018**, *3*, 7745–7756. [CrossRef]
28. Lu, Q.; Rosen, J.; Jiao, F. Nanostructured metallic electrocatalysts for carbon dioxide reduction. *ChemCatChem* **2015**, *7*, 38–47. [CrossRef]
29. Choudhury, J. New strategies for CO_2-to-methanol conversion. *ChemCatChem* **2012**, *4*, 609–611. [CrossRef]
30. Rodemerck, U.; Holeňa, M.; Wagner, E.; Smejkal, Q.; Barkschat, A.; Baerns, M. Catalyst development for CO_2 hydrogenation to fuels. *ChemCatChem* **2013**, *5*, 1948–1955. [CrossRef]
31. Meng, A.; Lin, L.; Yuan, X.; Shen, T.; Li, Z.; Li, Q. Ag/ZrO_2/MWCNT Nanocomposite as Non-Platinum Electrocatalysts for Enhanced Oxygen Reduction Reaction. *ChemCatChem* **2019**, *11*, 2900–2908. [CrossRef]
32. Zeng, L.; Zhao, T.; An, L. A high-performance supportless silver nanowire catalyst for anion exchange membrane fuel cells. *J. Mater. Chem. A* **2015**, *3*, 1410–1416. [CrossRef]
33. Holewinski, A.; Idrobo, J.; Linic, S. High-performance Ag–Co alloy catalysts for electrochemical oxygen reduction. *Nat. Chem.* **2014**, *6*, 828–834. [CrossRef] [PubMed]
34. Blizanac, B.; Ross, P.N.; Marković, N. Oxygen Reduction on Silver Low-Index Single-Crystal Surfaces in Alkaline Solution: Rotating Ring DiskAg (h kl) Studies. *J. Phys. Chem. B* **2006**, *110*, 4735–4741. [CrossRef]
35. Wiberg, G.K.; Mayrhofer, K.J.; Arenz, M. Investigation of the oxygen reduction activity on silver–a rotating disc electrode study. *Fuel Cells* **2010**, *10*, 575–581. [CrossRef]
36. Singh, P.; Buttry, D.A. Comparison of oxygen reduction reaction at silver nanoparticles and polycrystalline silver electrodes in alkaline solution. *J. Phys. Chem. C* **2012**, *116*, 10656–10663. [CrossRef]
37. Wang, Y.; Lu, X.; Liu, Y.; Deng, Y. Silver supported on Co3O4 modified carbon as electrocatalyst for oxygen reduction reaction in alkaline media. *Electrochem. Commun.* **2013**, *31*, 108–111. [CrossRef]
38. Lima, F.H.B.; de Castro, J.; Ticianelli, E.A. Silver-cobalt bimetallic particles for oxygen reduction in alkaline media. *J. Power Sources* **2006**, *161*, 806–812. [CrossRef]
39. Zafferoni, C.; Cioncoloni, G.; Foresti, M.; Dei, L.; Carretti, E.; Vizza, F.; Lavacchi, A.; Innocenti, M. Synergy of cobalt and silver microparticles electrodeposited on glassy carbon for the electrocatalysis of the oxygen reduction reaction: an electrochemical investigation. *Molecules* **2015**, *20*, 14386–14401. [CrossRef]
40. Yi, Q.; Chu, H.; Tang, M.; Yang, Z.; Chen, Q.; Liu, X. Carbon nanotube-supported binary silver-based nanocatalysts for oxygen reduction reaction in alkaline media. *J. Electroanal. Chem.* **2015**, *739*, 178–186. [CrossRef]
41. Yi, Q.; Song, L. Polyaniline-Modified Silver and Binary Silver-Cobalt Catalysts for Oxygen Reduction Reaction. *Electroanalysis* **2012**, *24*, 1655–1663. [CrossRef]
42. Fernández, J.L.; Walsh, D.A.; Bard, A.J. Thermodynamic guidelines for the design of bimetallic catalysts for oxygen electroreduction and rapid screening by scanning electrochemical microscopy. M− Co (M: Pd, Ag, Au). *J. Am. Chem. Soc.* **2005**, *127*, 357–365. [CrossRef] [PubMed]
43. Wang, Y.; Balbuena, P.B. Design of oxygen reduction bimetallic catalysts: ab-initio-derived thermodynamic guidelines. *J. Phys. Chem. B* **2005**, *109*, 18902–18906. [CrossRef] [PubMed]
44. Glavee, G.N.; Klabunde, K.J.; Sorensen, C.M.; Hadjapanayis, G.C. Borohydride reductions of metal ions. A new understanding of the chemistry leading to nanoscale particles of metals, borides, and metal borates. *Langmuir* **1992**, *8*, 771–773. [CrossRef]
45. Glavee, G.; Klabunde, K.; Sorensen, C.M.; Hadjipanayis, G. Sodium borohydride reduction of cobalt ions in nonaqueous media. Formation of ultrafine particles (nanoscale) of cobalt metal. *Inorg. Chem.* **1993**, *32*, 474–477. [CrossRef]
46. Bala, T.; Arumugam, S.K.; Pasricha, R.; Prasad, B.; Sastry, M. Foam-based synthesis of cobalt nanoparticles and their subsequent conversion to Co core Ag shell nanoparticles by a simple transmetallation reaction. *J. Mater. Chem.* **2004**, *14*, 1057–1061. [CrossRef]
47. Wu, H.; Zhang, C.; Jin, L.; Yang, H.; Yang, S. Preparation and magnetic properties of cobalt nanoparticles with dendrimers as templates. *Mater. Chem. Phys.* **2010**, *121*, 342–348. [CrossRef]
48. Lee, D.; Xia, Q.X.; Yun, J.M.; Kim, K.H. High-performance cobalt carbonate hydroxide nano-dot/NiCo $(CO_3)(OH)_2$ electrode for asymmetric supercapacitors. *Appl. Surf. Sci.* **2018**, *433*, 16–26. [CrossRef]
49. Gozdziewska, M.; Cichowicz, G.; Markowska, K.; Zawada, K.; Megiel, E. Nitroxide-coated silver nanoparticles: Synthesis, surface physicochemistry and antibacterial activity. *RSC Adv.* **2015**, *5*, 58403–58415. [CrossRef]

50. Chee, S.W.; Tan, S.F.; Baraissov, Z.; Bosman, M.; Mirsaidov, U. Direct observation of the nanoscale Kirkendall effect during galvanic replacement reactions. *Nat. Commun.* **2017**, *8*, 1224. [CrossRef]
51. Chung, H.T.; Won, J.H.; Zelenay, P. Active and stable carbon nanotube/nanoparticle composite electrocatalyst for oxygen reduction. *Nat. Commun.* **2013**, *4*, 1922. [CrossRef] [PubMed]
52. Zhu, X.; Gupta, K.; Bersani, M.; Darr, J.A.; Shearing, P.R.; Brett, D.J. lectrochemical reduction of carbon dioxide on copper-based nanocatalysts using the rotating ring-disc electrode. *Electrochim. Acta* **2018**, *283*, 1037–1044. [CrossRef]
53. Zhang, Y.; Liu, J.; Wu, G.; Chen, W. Porous graphitic carbon nitride synthesized via direct polymerization of urea for efficient sunlight-driven photocatalytic hydrogen production. *Nanoscale* **2012**, *4*, 5300–5303. [CrossRef] [PubMed]
54. Fageria, P.; Nazir, R.; Gangopadhyay, S.; Barshilia, H.C.; Pande, S. Graphitic-carbon nitride support for the synthesis of shape-dependent ZnO and their application in visible light photocatalysts. *RSC Adv.* **2015**, *5*, 80397–80409. [CrossRef]